Synthesis, FT-IR and NMR characterization, antimicrobial activity, cytotoxicity and DNA docking analysis of a new anthraquinone derivate compound

Sefa Celik, Funda Ozkok, Aysen E. Ozel, Yesim Müge Sahin, Sevim Akyuz, Belgi Diren Sigirci, Beren Basaran Kahraman, Hakan Darici & Erdal Karaoz

Taylor & Francis
Taylor & Francis Group

Check for updates

Synthesis, FT-IR and NMR characterization, antimicrobial activity, cytotoxicity and DNA docking analysis of a new anthraquinone derivate compound

Sefa Celik[a], Funda Ozkok[b], Aysen E. Ozel[c], Yesim Müge Sahin[d], Sevim Akyuz[e], Belgi Diren Sigirci[f], Beren Basaran Kahraman[f], Hakan Darici[g] and Erdal Karaoz[g]

[a]Engineering Faculty, Electrical–Electronics Engineering Department, Istanbul University-Cerrahpasa, Avcilar, Istanbul, Turkey; [b]Engineering Faculty, Department of Chemistry, Istanbul University-Cerrahpasa, Avcilar, Istanbul, Turkey; [c]Faculty of Science, Department of Physics, Istanbul University, Vezneciler, Istanbul, Turkey; [d]Department of Biomedical Engineering, Istanbul Arel University, Istanbul, Turkey; [e]Faculty of Science and Letters, Department of Physics, Istanbul Kultur University, Atakoy Campus, Istanbul, Turkey; [f]Faculty of Veterinary Medicine, Department of Microbiology, Istanbul University-Cerrahpasa, Avcilar, Istanbul, Turkey; [g]Faculty of Medicine, Department of Histology and Embryology, Istinye University, Istanbul, Turkey

Communicated by Ramaswamy H. Sarma

ABSTRACT

A new anthraquinone [1-(2-Aminoethyl)piperazinyl-9,10-dioxo-anthraquinone] derivative was synthesized and characterized by density functional theory (DFT) calculations, experimental and theoretical vibrational spectroscopy and NMR techniques. The most stable molecular structure of the title molecule was determined by DFT B3LYP method with 6-31++G(d,p) and 6-311++G(d,p) basis sets. The fundamental vibrational wavenumbers, IR and Raman intensities for the optimized structure of the investigated molecule were calculated and compared with the experimental vibrational spectra. The vibrational assignment of the molecule was done using the potential energy distribution analysis. The molecular electrostatic potential (MEP), highest occupied molecular orbital (HOMO) and lowest occupied molecular orbital (LUMO) were also calculated. The antibacterial activities of the new anthraquinone derivative against Gram-positive and Gram-negative bacteria were determined, and it was shown that the highest effectiveness was against *Staphylococcus aureus* and *S. epidermidis* while no activity was against Gram-negative bacteria. Moreover, the antimycotic activity of the title compound was examined and the cytotoxicity of anthraquinone derivate was determined. In order to find the possible inhibitory activity of the title compound, molecular docking of the molecule was carried out against DNA. The results indicated that the mentioned compound has a good binding affinity to interact with the DC3, DG4, DA5, DC21 and DC23 residues of DNA via the intermolecular hydrogen bonds.
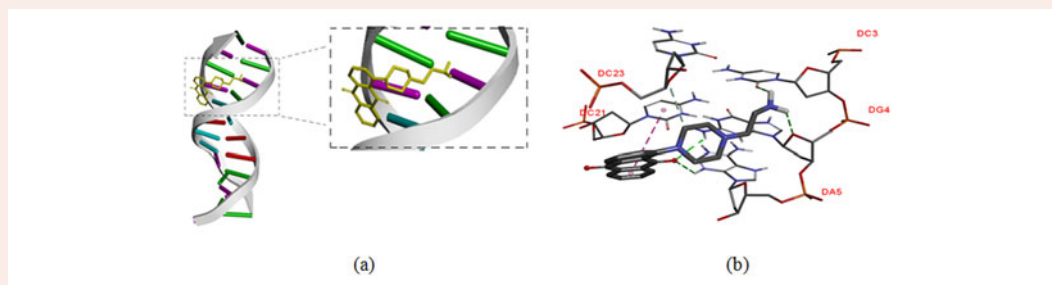
1. Introduction

Anthraquinone derivatives have a wide range of applications, such as being used as dyes, biologically active substances, medical agents, analytical reagents, indicators, data storage and processing devices, colorants in food, drugs, cosmetics, hair dyes, textiles, ground smoke-screens, pesticide, in pulp industry, purgative preparations, antiviral, antiparasitic, antioxidant, chelatant, diuretic, laxative, antimicrobial and antitumor drugs (Cudlin, Blumauerova, Steinerova, Mateju, & Zalabak, 1976; Driscoll, Hazard, Wood, & Goldin, 1974; Fain, 1999; IARC, 2013; Nollet & Gutierrez-Uribe, 2018; Sendelbach, 1989). Anthraquinones are also used to make seeds distasteful to birds (Windholtz, Budavari, Stroumtsos, & Fertig, 1976). The importance of anthraquinone derivatives is evident from their widespread application in industry and medicine, but little is known about the toxic or carcinogenic potential that

Figure 1. Schematic representation of the synthesis reaction of *1-(2-Aminoethyl)piperazinyl-9,10-dioxo-anthraquinone* (3) molecule.

these compounds may show to the human population (Sendelbach, 1989).

Various anthraquinones, substituted with hydroxyl, amino, halogen, carboxylic acid, aromatic group and sulfonate, have been tested against HIV-1 virus in human lymphocytes. Among the compounds tested, it has been found that the anthraquinones substituted with polyphenolic and/or polysulfonate have the strongest antiviral activity (Schinazi et al., 1990).

On the other hand, various amino anthraquinone derivatives hold potential among these applications. To give an example, Mitoxantrone molecule, an amino anthraquinone compound, is known as an anticancer chemotherapy drug.

In this study, antibacterial, antimicrobial and antimycotic activities, cytotoxicity, the conformational properties and structural and vibrational features of a new amino anthraquinone derivate [1-(2-Aminoethyl)piperazinyl-9,10-dioxo-anthraquinone], recently synthesized by our group, were investigated. The antimicrobial activities against Gram-positive and Gram-negative bacteria, antimycotic activities against yeast and fungi and cytotoxicity of anthraquinone derivate were determined. Moreover, molecular docking studies of the anthraquinone derivate to DNA were carried out for better understanding of the drug–receptor interaction.

2. Experimental and computational details

2.1. Synthesis

In a previous study of the group, a practical, one-step and economic synthesis method were developed to obtain amino and thio anthraquinone analogues (Ozkok & Sahin, 2016). In this study, the amino anthraquinone derivative [1-(2-Aminoethyl) piperazinyl-9,10-dioxo-anthraquinone] is synthesized by this novel method (Ozkok & Sahin, 2016) for biological applications. The starting material 1-Amino anthraquinone compound (1g) (1) and 25 ml ethylene glycol were stirred in the reaction flask, and then 1-(2-Aminoethyl)piperazine (0.53g) (2) was added. A yellowish mixture was obtained at the end. Later, 10 ml of aqueous potassium hydroxide solution was added to this yellowish mixture, and the reaction temperature was raised to 120–130 °C. After reflux (36 h), the red amino anthraquinone compound (3) was obtained (Figure 1). The new product was extracted with chloroform (30 ml). Organic layer was washed with water and dried with calcium sulfate. Synthesized novel

analogue was purified by column chromatography (Celik et al., 2018).

2.2. Antibacterial activity

The antibacterial activity of the (3) was examined by agar dilution method and the minimum inhibitory concentration (MIC) value was determined according to clinical and laboratory standards institute (formerly CLSI) (1). The antimicrobial activity was evaluated against Gram-positive (*Staphylococcus aureus* (ATCC 29213), *S. epidermidis* (ATCC 12228), *Enterococcus faecalis* (ATCC 29212), *Bacillus subtilis* (ATCC 6633)) and Gram-negative (*Escherichia coli* (ATCC 25922), *Klebsiella pneumoniae* (ATCC 4352), *Pseudomonas aeruginosa* (ATCC 27853), *Salmonella enteritidis* (KUEN 349)) bacteria. The strains were provided by the Faculty of Veterinary Medicine, Department of Microbiology Culture Collection, Istanbul University. Mueller–Hinton Agar (Fluka 70191) was used for the detection of the antibacterial effect and to maintain the strains. Mueller–Hinton broth (Fluka 90922) (CAMBH) with $MgCl_2\cdot2H_2O$ (10 mg Mg^{2+}/L) and $CaCl_2\cdot6H_2O$ (20 mg Ca^{2+}/L) was used as the medium for dilution. Test component was dissolved in 10 ml DMSO and prepared for a twofold step dilution for 10 serial dilutions between 0.009 and 5.1 mg/ml with CAMBH. 1 ml of each inoculum was poured to each Petri dish, and 9 ml Muller–Hinton agar brought to 45–50 °C was added to the inoculum and mixed with a circular dial until room temperature was reached. A bacterial suspension with 10^7 cfu/ml final concentration was prepared and was added into the microplate wells. The sterilized replicator with 3-mm pins, which deliver 2 μl, was placed into the microplate to soak the pins and transfer it onto the agar plate. The agars were incubated at 37 °C for 24 h. The MIC value was determined beyond the level where no inhibition of growth of test organisms was observed. Furthermore, Gentamicin sulfate (Sigma G1272) was used as the reference antibiotic standard. The experiments were conducted twice and data were averaged.

2.3. Antimycotic activity

The antimycotic effect of the (3) was examined with broth macro-dilution method according to CLSI (2). The antimycotic activities were evaluated against yeasts (*Candida albicans*, *Malassezia pachydermatis*) and fungi (*Microsporum canis*, *Trichophyton mentagrophytes*). The strains were provided by

Figure 2. Light microscopy photographs that were taken after a 48-h incubation with different concentrations of compound (3).

the Faculty of Veterinary Medicine, Department of Microbiology Culture Collection, Istanbul University.

A suspension equal to 0.5 McFarland turbidity in physiological salty water among 48-h yeast strains and 5 day fungi strains in Sabouraud Dextrose Agar (SDA) (Sigma S3181) was prepared in order to prepare the inoculum. The MIC of the compound was determined by twofold micro-dilution method in RPMI 1640 Medium (Sigma R8758) according to

CLSI (Sendelbach, 1989). Amphotericin B (Sigma 1032007) was used as the positive control. Testing was performed in test tubes in Sabouraud Dextrose Broth (SDB). The test tubes were incubated in a moist chamber at 25 °C for 7 days before being read. The lowest concentration that completely inhibits the reproduction and can be determined with the naked eye was recorded as the MIC value. The tests were duplicated and data were averaged.
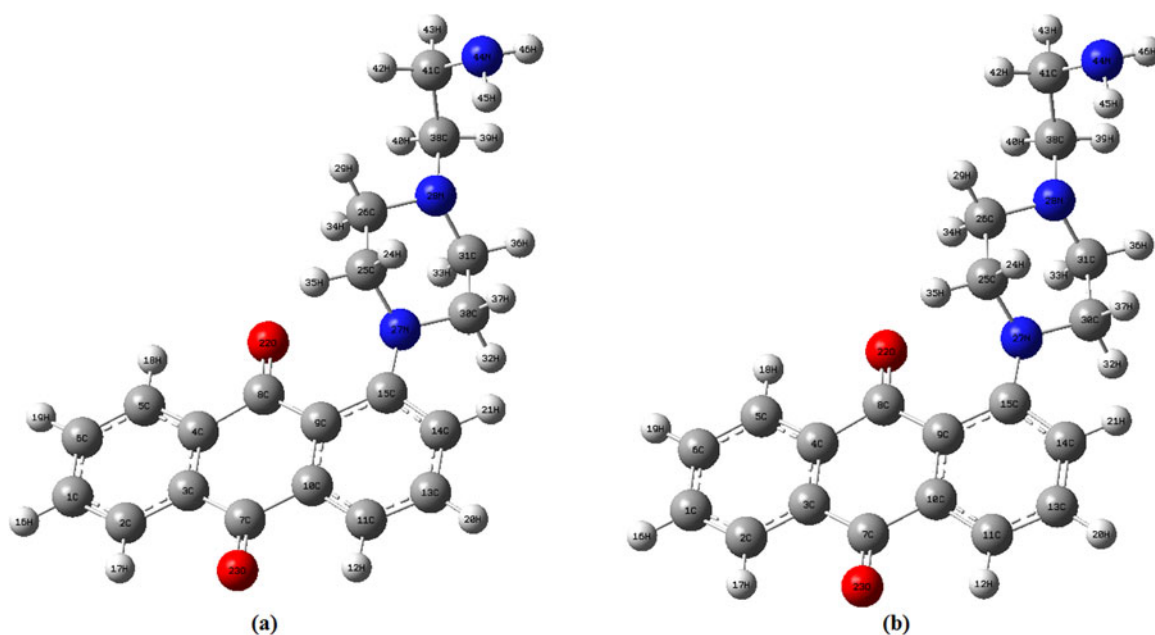
Figure 3. The most stable geometric structure of anthraquinone derivate calculated by DFT/B3LYP/6-31++G(d,p) (a) and DFT/B3LYP/6-311++G(d,p) (b) level of theories.

2.4. Light microscopy examinations

Mesenchymal stem cell line, which was obtained from the human umbilical cord (MSC) and A549 cancer cell line, was used. Volatile compounds used in the industry can cause cancer in the case of exhalation; therefore, the A549 cell line, derived from lung epithelial tumor, was chosen. During experiments, DMEM/F12 medium was used for MSCs, and RPMI 1640 was used for A549 cells. Each medium was supplemented with 10% fetal bovine serum and 1% penicillin/streptomycin. All culture media were purchased from GIBCO (BRL, Gaithersburg, MD, USA).

In the first stage of the study, cells were cultured with different concentrations of compound (**3**). In order to prepare several concentrations of the compound (**3**), 200 M main stock solution was prepared by solving amino anthraquinone in DMSO. Then, stock solution was solved in absolute ethanol to obtain 10 mM intermediate stock solutions. Lastly, the culture medium was used to dilute stock solutions. For the first experiments, both cell lines were cultured at the 100 nM, 1 μM, 10 μM, 100 μM, 1 mM and 10 mM concentrations for 48 h. After incubation, the cells were examined and photographed under a light microscope (Figure 2). As the concentration of the compound (**3**) increased, denser red color was observed.

2.5. Cytotoxicity analysis

Cytotoxicity analysis represents experiments that investigate whether compounds have lethal effects on cells or not. One of the most frequently used methods for this purpose depends on yellow-red formazan crystal formation according to live cell amount by using MTT or its modified version WST-1 for the living cells. Amount of the formed crystals was analyzed with spectrophotometer and results were compared with those of control group to identify any increase or decrease at the cell number. However, in this study, compound (**3**) causes similar reddish color of MTT or WST-1 methods. Consequently, MTT tests for compound (**3**) can be illusive because it can give similar spectrophotometry results even if MTT was not used. As a result, xCELLigence system was used in order to confirm the results of MTT/WST-1. The xCELLigence method allows real-time viability determination of cells in culture wells with gold microelectrodes at the base of culture plate. Electrodes transmit electrical currents at very small voltages into the culture plates to determine the impedance differences. xCELLigence collects and processes the obtained data on the computer in the form of cell index (CI).

2.6. xCELLigence analysis

To test the precision of the xCELLigence system, 100 μl culture medium was added to each well of the special 16-well plate and the system was run. Then, 2.5×10^4, 5×10^4, 10×10^4, 20×10^4 and 40×10^4 cells with 100 μl culture medium were added and incubated for 72 h by taking a measurement for every 10 min. According to analysis, it has been found that CI results were related to cultured cell number. The most appropriate cell number per well was determined as 2×10^5 for a 72-h experiment as being consistent with the literature. 20,000 cells were added within 100 μl culture medium. Then, 50 μl compound (**3**) with different concentrations, which were 100 nM, 1 μM, 10 μM, 100 μM and 1 mM concentrations for MSCs, and 10, 50 100, 200 and 500 μM concentrations were used for A549 cells. Each concentration was evaluated at least in triplicate except for 1 mM concentration.

The final measurement before the addition of compound during the analysis was accepted as 'baseline', and the CI was calculated as 1 at this point. During the analysis, the cells were monitored for 72 h and calculations were taken

Table 1. Antimicrobial activity of (3) with minimum inhibitory concentrations (µg/ml).

	Minimum inhibitory concentrations (MIC) in µg/ml							
	Gram-positive bacteria				Gram-negative bacteria			
Compounds	S. aureus	S. epidermidis	E. faecalis	B. subtilis	E. coli	K. pneumoniae	P. aeruginosa	S. enteritidis
(3)	63.75	63.75	(−)	510	(−)	(−)	(−)	(−)
Gentamicin	0.5	0.5	0.8	0.5	0.25	0.25	0.25	0.25

(−), MIC value was not detected in the test concentrations.

Table 2. Antimycotic activity of (3) with MIC values.

	Minimum inhibitory concentrations (MIC) in µg/ml			
	Yeasts		Fungi	
Compounds	C. albicans	M. pachydermatis	M. canis	T. mentagrophytes
(3)	15.93	63.75	255	255
Amphotericin B	0.125	0.125	0.125	0.125
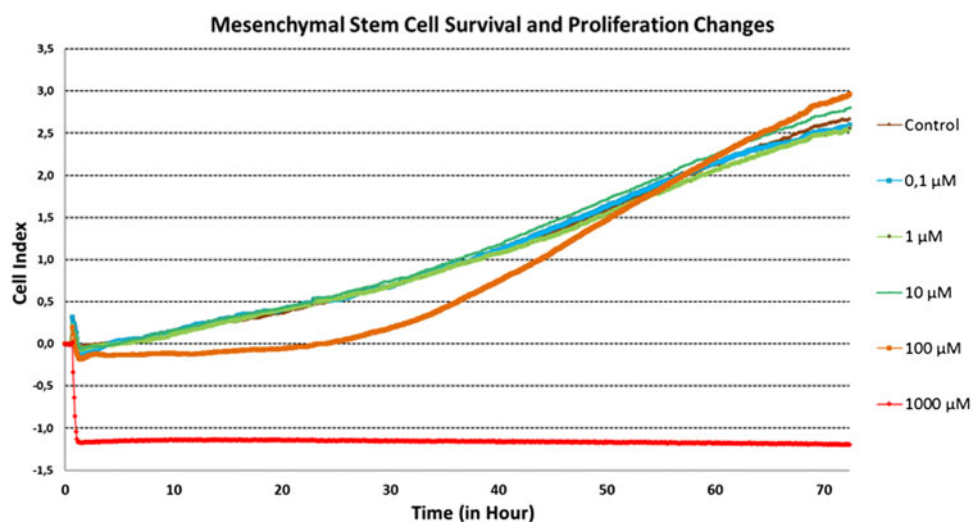
Figure 4. xCELLigence MSC proliferation curves. No difference was observed between controls up to 10 µM concentration. Orange lines show the proliferation delay caused by 100 µM compound. Cells compensated this delay and reached control levels at the end of 72 h of experiment. The red line represents cells that were exposed to 1 mM compound (3). Each curve represents average values of the triplicate experiments (except 1000 µM).
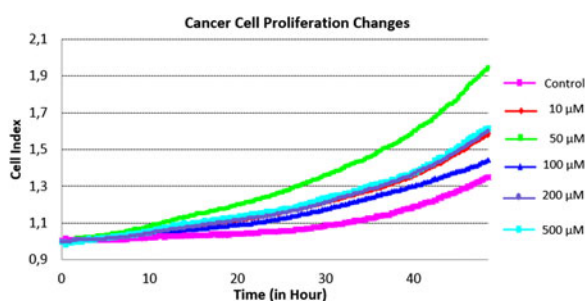
Figure 5. xCELLigence A549 cancer cell proliferation curves. All groups show increase in cell number. Each curve represents average values of the triple experiments (except 500 µM).

every 5 min. Impedance measurements after compound addition revealed real-time interactions dependent on concentration in cells.

2.7. WST analysis

Simultaneously with the xCELLicence analysis, MTT-based WST-1 analysis was performed. In the assays, 5000 cells per well were used for the 96-well plate. Compound (3) was evaluated at the same concentrations with the xCELLicence analysis. Cells without compound were used as positive control and same concentrations of the compound without cells were used to evaluate background interference. Cells were cultured for 72 h with the compound. 10 µl of WST-1 solution was added to the wells according to the manufacturer's instructions. The mixture was shaken on the orbital shaker after the addition of the chemicals and before measurement for 1 min. The measurements were taken 2 h after mixing. Measurements were made at 450 nm wavelength on a Spectrostar Nano instrument, and the results were analyzed and plotted in an MS Excel file.

2.8. Experimental and computational studies

The ATR-FT-IR spectrum of the investigated sample was recorded on a Bruker Tensor FT-IR spectrometer with a diamond ATR unit. In order to analyze overlapping bands, we performed band component analysis. The band-fitting procedures were performed using GRAMS/AI 7.02 (Thermo Electron Corporation, Waltham, MA) software package. Band fitting was done using a Voigt function; the fitting was

Table 3. Structural parameters for monomeric form of new anthraquinone compound obtained by DFT/B3LYP (6-311++G(d,p)) in gas phase.

Atoms	Mono[a]	Nakagawa (2017)	Wnuk (2012)	Atoms	Mono[a]	Wnuk (2012)	Atoms	Mono[a]	Nakagawa (2017)	Wnuk (2012)	Atoms	Mono[a]	Nakagawa (2017)	Atoms	Mono[a]	Atoms	Mono[a]
R(1,2)	1.389	1.379	1.374	R(15,27)	1.393	1.3943	A(2,1,6)	119.9	120.7	119.84	A(10,9,15)	118.5	120.3	A(28,26,29)	109.2	A(39,38,41)	108.3
R(1,6)	1.399	1.382	1.380	R(24,25)	1.102	0.97	A(2,1,16)	120.0	119.6	120.1	A(7,10,9)	122.3	119.28	A(28,26,34)	111.4	A(40,38,41)	109.7
R(1,16)	1.084	0.95	0.93	R(25,26)	1.523	1.5094	A(6,1,16)	120.1	119.6	120.1	A(7,10,11)	116.1	122.03	A(29,26,34)	108.1	A(38,41,42)	109.9
R(2,3)	1.399	1.392	1.3934	R(25,27)	1.469	1.4634	A(1,2,3)	120.0	120.09	119.96	A(9,10,11)	121.6	118.68	A(15,27,25)	119.3	A(38,41,43)	108.5
R(2,17)	1.083	0.95	0.93	R(25,35)	1.085	0.97	A(1,2,17)	121.5	120.0	120.0	A(10,11,12)	118.6		A(25,27,30)	119.2	A(38,41,44)	115.5
R(3,4)	1.401	1.393	1.3919	R(26,28)	1.467	0.97	A(3,2,17)	118.5	120.0	120.0	A(10,11,13)	119.5	119.36	A(26,28,31)	111.3	A(42,41,43)	105.9
R(3,7)	1.482	1.489	1.4766	R(26,29)	1.092	0.97	A(2,3,4)	120.3	119.21	120.37	A(12,11,13)	121.8		A(26,28,38)	109.7	A(42,41,44)	108.1
R(4,5)	1.399	1.397	1.3905	R(26,34)	1.102	1.4608	A(2,3,7)	119.7	119.08	119.92	A(11,13,14)	120.2	121.52	A(31,28,38)	112.7	A(43,41,44)	108.5
R(4,8)	1.501	1.471	1.4936	R(27,30)	1.462	1.5094	A(4,3,7)	120.0	121.71	119.68	A(11,13,20)	120.2	119.2	A(27,30,31)	112.7	A(41,44,45)	109.2
R(5,6)	1.390	1.376	1.379	R(28,31)	1.461	0.97	A(3,4,5)	119.3	120.12	118.82	A(14,13,20)	119.5	119.2	A(27,30,32)	109.9	A(41,44,46)	110.6
R(5,18)	1.083	0.95	0.93	R(28,38)	1.528	0.97	A(3,4,8)	118.5	120.16	119.68	A(13,14,15)	122.1	120.52	A(27,30,37)	109.1	A(45,44,46)	106.8
R(6,19)	1.084	0.95	0.95	R(30,31)	1.092	0.97	A(5,4,8)	120.2	119.72	118.81	A(15,14,21)	118.7	119.7	A(31,30,37)	111.8		
R(7,10)	1.499	1.487	1.4917	R(30,32)	1.103		A(4,5,6)	118.5	119.9	120.26	A(9,15,14)	119.1	119.7	A(32,30,37)	108.7		
R(7,23)	1.221	1.2172	1.2176	R(30,37)	1.105		A(4,5,18)	120.3	120.0	119.9	A(9,15,27)	117.8	119.56	A(28,31,30)	108.8		
R(8,9)	1.487	1.468	1.4873	R(31,33)	1.094		A(1,6,5)	120.3	119.97	120.67	A(14,15,27)	123.0		A(28,31,33)	108.4		
R(8,22)	1.224	1.2449	1.2171	R(31,36)	1.096		A(1,6,19)	119.9	120.0	119.7	A(24,25,26)	119.1		A(30,31,33)	111.0		
R(9,10)	1.420	1.424	1.4142	R(38,39)	1.106		A(5,6,19)	119.8	120.0	119.7	A(24,25,27)	109.2		A(30,31,36)	111.7		
R(9,15)	1.434	1.404	1.4257	R(38,40)	1.537		A(3,7,10)	117.7	118.0	118.10	A(24,25,35)	108.9		A(33,31,36)	108.8		
R(10,11)	1.391	1.407	1.3804	R(38,41)	1.095		A(3,7,23)	121.3	119.34	121.14	A(26,25,27)	108.4		A(28,38,39)	108.8		
R(11,12)	1.082	0.93	0.93	R(41,42)	1.095		A(10,7,23)	121.0	122.65	120.74	A(26,25,35)	110.9		A(28,38,40)	108.6		
R(11,13)	1.390	1.406	1.3707	R(41,43)	1.463		A(4,8,9)	118.4	118.98	118.32	A(27,25,35)	109.4		A(39,38,40)	107.8		
R(13,14)	1.385	1.365	1.3722	R(41,44)	1.016		A(4,8,22)	118.4	120.02	118.45	A(25,26,28)	110.0					
R(13,20)	1.085	0.95	0.93	R(44,45)	1.016		A(9,8,22)	123.2	120.98	123.2	A(25,26,29)	110.7					
R(14,15)	1.412	1.393	1.4020	R(44,46)			A(8,9,10)	118.7	121.36	117.97	A(25,26,34)	108.5					
R(14,21)	1.081	0.95	0.93	A(6,5,18)	121.3	119.9	A(8,9,15)	122.4	118.34	123.22							

[a]R and A stand for bond (Å) and angle (deg), respectively.

undertaken until reproducible, and converged results were obtained with squared correlations greater than $r^2 \sim 0.99999$.

The most stable conformation of the (3) was determined by the Spartan06 program (Shao et al., 2006) using density functional theory (DFT), B3LYP functional, 6-31++G(d,p) and 6-311++G(d,p) basis sets (Becke, 1993). Afterwards, the stable geometry with the lowest molecular energy was calculated by Gaussian03 program (Frisch et al., 2004) using DFT/B3LYP level and both 6-31++G(d,p) and DFT/B3LYP/6-311++G(d,p) basis sets. The optimized geometric structures of the title molecule using DFT/B3LYP/6-31++G(d,p) and DFT/B3LYP/6-311++G(d,p) level of theories are shown in Figure 3. The harmonic force field for the title molecule was calculated with the scaled quantum mechanical force field procedure of Pulay, Fogarasi, Pongor, Boggs, and Vargha, (1983).

By using the Molvib program, the force fields in the Cartesian coordinates were converted into natural internal coordinates, and the IR intensities, Raman activities and the potential energy distributions (PEDs) of the vibration modes were calculated (Sundius, 1990, 2002). The Raman intensity of the molecule was calculated using the Simirra simulation program, which transformed Raman activities into intensity (Istvan, 2002). Lorentzian band shapes with bandwidth (FWHM) of $10\,cm^{-1}$ were used in the simulations.

The following scale factors for both DFT/B3LYP/6-31++G(d,p) and DFT/B3LYP/6-311++G(d,p) level of calculations were chosen to give the best fit to the experimental data:

N–H stretch	0.89
C–H stretch	0.93
N–H and C–H deformations	0.92
C=O stretch	0.90
All others	0.98

3. Results and discussion

The chemical structure of new anthraquinone derivative (3) was identified by spectroscopic methods. Red oil, Yield: 0.58 g (42%) R_f [(Petroleum ether/Dichloromethane) (1:1)]: 0.49. UV-vis(CHCl$_3$): λ_{max} ($\log\varepsilon$) = 3.65 (373 nm), 4.53 (255 nm). ^{1}H NMR (499.74 MHz, CDCl$_3$): $\delta = 4.13$-4.14 (m, 2 H, H$_{pip}$), 4.19-4.20 (m, 2 H, H$_{pip}$), 4.15-4.16 (m, 2 H, H$_{CH2}$), 4.17-4.18 (m, 2 H, H$_{CH2}$), 2.30 (s, 2 H, H$_{NH2}$), 7.22-8.25 (m, 7 H, H$_{arom}$). ^{13}C NMR (125.66 MHz, CDCl$_3$): $\delta = 37.75$ (**CH$_2$**-NH$_2$), 63.11, 63.57 (C$_{pip.}$), 66.78 (**CH$_2$**-CH$_2$-NH$_2$), 115.17, 116.28, 118.54, 131.47, 132.16, 133.16, 133.65, 135.72, 161.59 (C$_{arom}$ and CH$_{arom}$), 181.40 (C=O). MS [+ESI]: $m/z = 335.90$ [M + H]$^+$, C$_{20}$H$_{21}$N$_3$O$_2$, (M, 335.20 a.u.).

The mass spectra were recorded on (Shimadzu) LCMS-8045 triple quadrupole spectrometer in ESI (+) polarity. The MS spectrum is shown as supplementary file, Figure S1. The formation of molecular ion {[M + H]$^+$ (m/z 335.90)} and fragment ion peaks {[M-NH$_2$-CH$_2$]$^+$ and [M-NH$_2$-CH$_2$-CH$_2$]$^+$} confirms the molecular formula.

Table 4. The observed and calculated wavenumbers of [1-(2-Aminoethyl)piperazinyl-9,10-dioxo-anthraquinone] in comparison with the experimental and theoretical vibrational wavenumbers of 9,10-anthraquinone (Gribov et al.,1993).

9,10-Anthraquinone (Gribov et al.,1993)		(3) This study	B3LYP/ 6-31++g(d,p)			B3LYP/ 6-311++g(d,p)			PED% 6-311++G(d,p)
Exp.	Theoretical	ATR-FTIR	ν_{cal}^{s}	I(IR)	I(Ra)	ν_{cal}^{s}	I(IR)	I(Ra)	
		3478	3374	4	3	3362	5	3	$\nu_{NH}(97)$
		3371							
		3238	3294	1	9	3290	1	9	$\nu_{NH}(100)$
		3133	3116	10	27	3098	9	28	$\nu_{CH}(99)$
			3113	2	29	3095	1	30	$\nu_{CH}(99)$
			3109	11	28	3091	10	29	$\nu_{CH}(96)$
			3105	4	22	3087	4	23	$\nu_{CH}(99)$
3081	3068		3088	16	26	3071	13	26	$\nu_{CH}(95)$
	3061		3077	13	24	3059	12	25	$\nu_{CH}(91)$
3068	3059		3074	4	23	3056	3	22	$\nu_{CH}(93)$
	3057		3068	7	12	3053	7	16	$\nu_{CH}(98)$(asym.)
		3029	2990	18	10	2976	18	10	$\nu_{CH}(96)$(asym.)
			2984	32	12	2969	31	12	$\nu_{CH}(93)$(asym.)
			2972	66	15	2956	72	17	$\nu_{CH}(95)$(asym.)
		2957	2962	43	18	2948	38	19	$\nu_{CH}(91)$(asym.)
			2943	34	9	2931	32	9	$\nu_{CH}(95)$(asym.)
		2918	2933	17	17	2919	14	17	$\nu_{CH}(98)$(sym.)
			2871	85	5	2860	85	5	$\nu_{CH}(95)$(sym.)
		2852	2857	48	28	2845	42	29	$\nu_{CH}(96)$(sym.)
			2849	82	15	2838	79	16	$\nu_{CH}(94)$(sym.)
			2828	77	19	2816	75	20	$\nu_{CH}(97)$(sym.)
			2813	60	10	2803	54	10	$\nu_{CH}(97)$(sym.)
1681	1671	1668	1658	139	50	1651	154	46	$\nu_{CO}(51)+ \delta_{CCC}(13)$
			1642	103	100	1634	103	100	$N_{CO}(37)+ \delta_{CCC}(13)+ \nu_{CC}(12)$
			1608	72	64	1600	72	62	$\nu_{CC}(40)$
		1629	1601	26	35	1598	22	58	$\delta_{HNH}(94)$
1594	1595	1595	1598	174	36	1591	177	38	$\nu_{CC}(53)$
			1592	49	58	1585	54	59	$\nu_{CO}(32)+ \nu_{CC}(30)$
1575	1573	1571	1570	77	15	1562	82	15	$\nu_{CC}(45)+ \nu_{CO}(12)+ \delta_{CCH}(8)+ \delta_{CCC}(7)$
			1476	2	5	1470	2	5	$\delta_{CCH}(41)+ \nu_{CC}(34)$
1475	1472	1470	1462	48	5	1456	45	6	$\nu_{CN}(12)+ \delta_{CCH}(20)+ \nu_{CC}(16)+ \delta_{HCH}(7)$
		1447	1452	9	7	1448	10	7	$\delta_{HCH}(83)$
1455	1441		1448	13	7	1443	13	7	$\delta_{CCH}(32)+ \nu_{CC}(30)$
			1437	13	13	1434	9	12	$\delta_{HCH}(96)$
			1436	30	13	1432	31	12	$\delta_{HCH}(59)+ \nu_{CC}(7) + \delta_{CCH}(5)$
		1430	1431	1	10	1429	2	10	$\delta_{HCH}(93)$
			1428	39	8	1425	21	9	$\delta_{HCH}(58)+ \nu_{CC}(9)$
		1415	1425	34	9	1421	32	10	$\delta_{HCH}(64)+ \nu_{CC}(9)$
		1401	1419	14	12	1416	32	12	$\delta_{HCH}(53)+ \delta_{CCH}(9)+ \nu_{CC}(5)$
		1380	1379	101	9	1375	88	9	$\nu_{CN}(13)+ \delta_{NCH}(20)+ \delta_{CCH}(13)+ \nu_{CC}(7)$
			1374	58	13	1371	61	12	$\delta_{NCH}(40)+ \nu_{CN}(10)+ \delta_{CCH}(13)$
1370	1371		1360	7	7	1356	4	4	$\delta_{CCH}(36)+ \delta_{NCH}(25)+ \nu_{CC}(9)$
			1359	2	7	1343	1	5	$\nu_{CC}(79)$
			1356	19	7	1352	14	5	$\delta_{NCH}(29)+ \delta_{CCH}(21)+ \nu_{CC}(5)$
		1342	1342	18	6	1336	34	7	$\delta_{CCH}(25)+ \delta_{NCH}(7)+ \nu_{CC}(12)$
			1334	40	7	1334	15	7	$\delta_{CCH}(57)+ \delta_{CNH}(12)$
			1328	31	9	1325	25	7	$\delta_{CNH}(10)+ \delta_{CCH}(43)+ \delta_{NCH}(9)$
			1324	24	10	1320	41	12	$\delta_{NCH}(32)+ \nu_{CC}(8)+ \delta_{CCH}(5)$
			1312	2	6	1311	4	7	$\delta_{NCH}(42)+ \delta_{CCH}(36)$
1330	1316	1314	1300	206	6	1295	179	6	$\nu_{CC}(35) + \delta_{CCO}(7) + \delta_{CCC}(8) + \delta_{CCH}(12)$
			1285	7	6	1283	8	6	$\delta_{NCH}(36) + \nu_{CN}(10) + \delta_{CCH}(7)$
1287	1288		1273	57	18	1272	27	10	$\delta_{CCH}(47) + \delta_{NCH}(16) + \nu_{CN}(7)$
		1266	1270	355	21	1263	377	19	$\nu_{CC}(33) + \delta_{NCH}(6) + \delta_{CCO}(5)$
		1241	1242	30	4	1241	35	4	$\delta_{NCH}(19) + \delta_{CCH}(17) + \delta_{CCC}(9)$
			1230	127	8	1228	142	8	$\delta_{NCH}(20) + \delta_{CCH}(8) + \nu_{CN}(12)$
			1227	16	9	1225	15	9	$\delta_{NCH}(20) + \delta_{CCH}(25) + \delta_{CCC}(5)$
		1199	1204	61	5	1201	70	5	$\nu_{CN}(7) + \delta_{NCH}(7) + \nu_{CC}(6) + \delta_{CNH}(5)$
1173	1167	1186	1185	11	24	1183	6	22	$\delta_{CCH}(23) + \nu_{CC}(18) + \delta_{CCC}(8) + \delta_{NCH}(7)$
			1181	18	20	1181	22	22	$\delta_{CCH}(39) + \delta_{NCH}(30)$
			1168	17	34	1165	16	31	$\delta_{CCH}(63) + \nu_{CC}(9)$
		1156	1157	14	37	1154	13	40	$\nu_{CN}(36) + \delta_{NCH}(11)$
1146	1160	1142	1152	21	31	1150	26	36	$\delta_{CCH}(28) + \delta_{CCC}(21) + \nu_{CC}(11)$
			1141	35	23	1139	29	24	$\nu_{CN}(35) + \delta_{CCH}(24) + \delta_{CNC}(7)$
			1139	8	23	1137	14	26	$\delta_{CCH}(53) + \nu_{CN}(6) + \nu_{CC}(5)$
			1120	9	5	1118	10	5	$\nu_{CN}(39) + \delta_{CCH}(10) + \delta_{CNH}(9) + \nu_{CC}(7)$
			1100	18	17	1097	18	17	$\delta_{NCH}(18) + \nu_{CN}(8) + \Gamma_{CNCC}(8) + \delta_{CCH}(8) + \nu_{CC}(6)$

Table 4. Continued.

9,10-Anthraquinone (Gribov et al.,1993)		(3) This study						
Exp.	Theoretical	ATR-FTIR	B3LYP/ 6-31++g(d,p)			B3LYP/ 6-311++g(d,p)		PED% 6-311++G(d,p)
1096	1090	1109	1091	3	28	1090 4 21		$\delta_{CCC}(30) + \delta_{CCH}(27) + \nu_{CC}(16)$
			1086	13	48	1083 17 50		$\nu_{CC}(39) + \delta_{CCH}(15)$
		1072	1081	13	26	1078 14 26		$\nu_{CN}(20) + \delta_{NCH}(21) + \Gamma_{CNCC}(6)$
			1068	6	7	1066 6 7		$\delta_{CCC}(10) + \nu_{CC}(13) + \delta_{NCH}(8) + \delta_{CNC}(6) + \delta_{CCH}(5)$
		1051	1042	6	20	1040 6 20		$\delta_{CCH}(30) + \delta_{NCH}(25)$
1034	1030	1034	1037	11	35	1035 11 36		$\nu_{CC}(48) + \delta_{CCH}(24)$
			1028	13	14	1025 13 14		$\nu_{CC}(30) + \delta_{NCH}(17) + \delta_{CCH}(6)$
			1007	0	5	1006 0 5		$\Gamma_{CCCH}(86) + \Gamma_{CCCC}(12)$
		996	1005	35	5	1002 34 6		$\delta_{CCH}(10) + \delta_{CNC}(9) + \nu_{CN}(7) + \nu_{CC}(6) + \Gamma_{CCCH}(9)$
			995	2	2	998 5 4		$\Gamma_{CCCH}(78) + \Gamma_{CCCC}(9)$
970	971	962	989	2	2	992 2 2		$\Gamma_{CCCH}(90) + \Gamma_{CCCC}(6)$
			986	65	2	985 64 2		$\delta_{CNH}(11) + \nu_{CN}(12) + \delta_{CCH}(18) + \nu_{CC}(10) + \delta_{NCH}(5)$
		942	945	38	1	944 38 1		$\nu_{CC}(23) + \nu_{CN}(9) + \delta_{CNC}(6) + \delta_{NCH}(5) + \Gamma_{CCCH}(6)$
935	930	924	925	64	2	925 48 3		$\Gamma_{CCCH}(47) + \delta_{CCO}(6)$
			922	6	3	923 13 3		$\Gamma_{CCCH}(33) + \delta_{CCC}(21) + \delta_{CCO}(8)$
			912	33	8	911 47 9		$\delta_{CCO}(18) + \delta_{CCC}(23) + \nu_{CC}(26)$
		906	907	0	4	906 0 5		$\Gamma_{CCCH}(83)$
		879	879	70	3	879 69 3		$\Gamma_{CNHH}(30) + \delta_{CCH}(16) + \delta_{NCH}(11) + \delta_{CNH}(9) + \nu_{CC}(7)$
		859	856	4	4	855 9 4		$\delta_{NCH}(23) + \delta_{CCH}(13) + \nu_{CC}(7) + \delta_{CCN}(9) + \Gamma_{CNCC}(5)$
			851	126	3	849 121 3		$\Gamma_{CNHH}(40) + \nu_{CN}(25) + \nu_{CC}(14)$
		834	835	29	2	829 6 2		$\delta_{CCH}(11) + \delta_{NCH}(16) + \Gamma_{CCCC}(13) + \Gamma_{CCCN}(7) +\Gamma_{CCCH}(7)$
			827	10	2	835 26 3		$\Gamma_{CCCC}(25) + \Gamma_{CCCH}(15) + \Gamma_{CCCN}(8) + \Gamma_{CCCO}(7)$
			809	2	3	809 0 2		$\delta_{CCC}(22) + \nu_{CN}(7)+ \nu_{CC}(6) + \Gamma_{CCCO}(8)$
815	819	804	808	20	3	808 25 2		$\Gamma_{CCCO}(24) + \Gamma_{CCCH}(25)$
792	792	763	787	9	1	788 9 1		$\Gamma_{CCCC}(26) + \Gamma_{CCCO}(12) + \Gamma_{CCCH}(34)$
			763	3	4	763 3 4		$\delta_{CCC}(33) + \nu_{CN}(14)$
			747	5	6	747 5 5		$\delta_{CCH}(12) + \nu_{CN}(26) + \Gamma_{CCCC}(7)$
			741	33	8	741 26 7		$\Gamma_{CCCC}(24) + \Gamma_{CCCH}(10) + \Gamma_{CCCN}(10) + \Gamma_{CCCO}(6)$
693	696	719	720	47	1	720 54 1		$\Gamma_{CCCC}(43) + \Gamma_{CCCH}(17) + \Gamma_{CCCO}(17)$
	680		693	2	1	696 1 1		$\delta_{CCC}(37) + \delta_{CCO}(32) + \Gamma_{CCCC}(6)$
		676	670	6	7	671 6 6		$\Gamma_{CCCC}(54) + \Gamma_{CCCO}(11) + \Gamma_{CCCN}(9)$
		652	666	13	11	666 14 10		$\delta_{CCC}(41) + \delta_{CNC}(5) + \nu_{CC}(6)$
			632	2	22	633 3 21		$\delta_{CNC}(13) + \delta_{CCC}(34) + \Gamma_{CNCC}(6)$
624	594	617	619	4	4	620 4 4		$\delta_{CCC}(70)$
		582	571	8	5	570 9 5		$\Gamma_{CCCC}(43) + \Gamma_{CCCN}(19) + \delta_{CNC}(7)$
		560	541	2	4	540 2 4		$\delta_{CCN}(26) + \delta_{CNC}(18) + \delta_{CCH}(8)$
		528	506	5	5	505 5 5		$\delta_{CCN}(25) + \Gamma_{CCCC}(6)$
			493	5	13	492 5 13		$\Gamma_{CCCC}(59) + \delta_{CCN}(5)$
			489	0	16	488 0 17		$\delta_{CCN}(34) + \Gamma_{CCCC}(10)$
			480	1	26	480 1 25		$\delta_{CCC}(45) + \delta_{CCN}(19)$
		471	467	3	83	467 2 82		$\delta_{CCC}(39) + \delta_{CCN}(19)$
		452	435	2	5	432 2 5		$\Gamma_{CCCC}(68) + \Gamma_{CCCO}(5)$
			427	0	5	425 0 6		$\Gamma_{CCCC}(76)$
		419	418	7	9	416 6 10		$\Gamma_{CNCC}(42) + \delta_{CNC}(17) + \delta_{CCC}(8)$
		400	408	5	14	407 6 13		$\delta_{CCO}(15) + \Gamma_{CNCC}(28) + \nu_{CC}(9) + \Gamma_{CCCC}(6)$
390	377	381	394	23	6	393 21 7		$\delta_{CCO}(29) + \delta_{CCC}(10) + \nu_{CC}(11) + \delta_{CCN}(5)$
375	358	369	369	5	5	367 5 5		$\delta_{CNC}(23) + \delta_{CCN}(20) + \Gamma_{NCCH}(10) + \Gamma_{CNCC}(6) + \delta_{NCH}(5)$
		359	350	2	4	349 2 4		$\delta_{CCC}(25) + \Gamma_{CNCC}(12) + \nu_{CC}(6)$
			335	5	10	333 6 10		$\Gamma_{CNCC}(66)$
			319	2	7	319 1 8		$\Gamma_{CCCC}(23) + \delta_{CCC}(13) + \delta_{CNC}(12) + \Gamma_{CNCC}(9)$
			307	4	3	306 3 3		$\Gamma_{CNCC}(21) + \delta_{CCC}(11) + \delta_{CNC}(14) + \Gamma_{CCNH}(6)$
			281	12	3	279 12 3		$\Gamma_{CCNH}(34) + \Gamma_{CNCC}(13) + \delta_{CCC}(7)+ \delta_{CNC}(8)$
			265	17	18	263 16 18		$\Gamma_{CNCC}(22) + \Gamma_{CCNH}(17) + \Gamma_{CCCC}(25)$
237	255		230	0	26	229 0 26		$\delta_{CNC}(15) + \delta_{CCC}(10) + \nu_{CC}(15) + \nu_{CN}(7) + \Gamma_{CNCC}(6)$
			227	15	24	226 14 22		$\Gamma_{CCNH}(28) + \delta_{CCN}(21) + \Gamma_{CNCC}(7)$
			214	9	33	211 10 32		$\Gamma_{CCCC}(52) + \Gamma_{CNCC}(8)$
			186	1	11	185 1 12		$\Gamma_{CCCC}(26) + \delta_{CNC}(9) + \delta_{CCN}(7) + \delta_{CCC}(6) + \Gamma_{NCCH}(5)$
167	146		164	1	11	163 1 12		$\Gamma_{CCCC}(29) + \Gamma_{CNCC}(21) + \Gamma_{NCCH}(11)$
			154	5	17	152 5 16		$\Gamma_{CNCC}(26) + \Gamma_{CCCC}(33)$
			140	1	13	139 1 13		$\Gamma_{CNCC}(35) + \Gamma_{CCCC}(16) + \Gamma_{NCCH}(7)$
			112	0	17	110 0 18		$\Gamma_{CCCC}(78)$
			92	2	73	91 2 74		$\Gamma_{CNCC}(49) + \Gamma_{CCCC}(8) + \delta_{CNC}(6) + \Gamma_{CNCH}(5)$
			72	0	40	72 0 43		$\Gamma_{CNCC}(38) + \delta_{CNC}(9)+ \Gamma_{NCCH}(7) + \delta_{CCN}(12)$
			51	1	68	52 1 65		$\Gamma_{CNCH}(31) + \Gamma_{NCCH}(15)+ \Gamma_{CCCC}(16) + \Gamma_{CNCC}(13)$
			41	3	154	40 3 183		$\Gamma_{CCCC}(43) + \Gamma_{CNCH}(14)$
			30	1	670	31 1 650		$\Gamma_{CNCC}(45) + \Gamma_{CCCC}(25)$
			23	2	586	23 2 601		$\Gamma_{CNCC}(45) + \Gamma_{CCCC}(29)$

$\nu_{cal}{}^{s}$ = Scaled calculated wavenumbers.
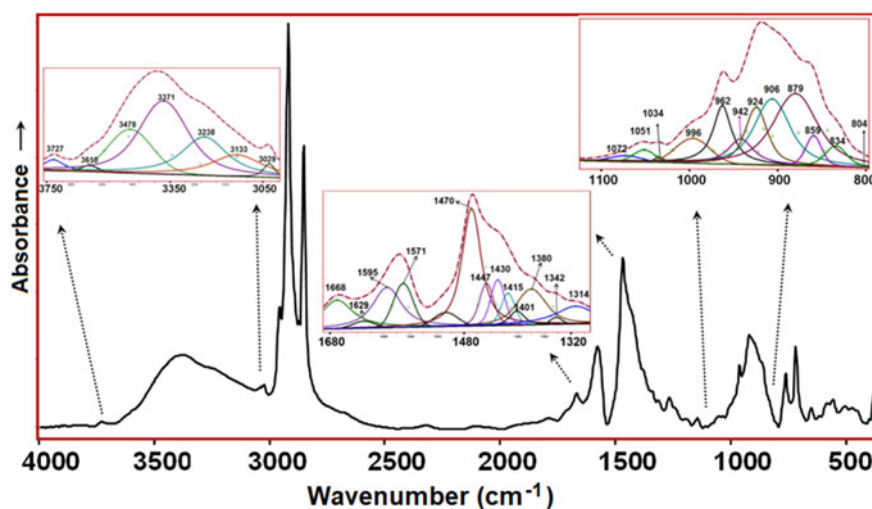
Figure 6. The experimental FT-IR spectrum of new anthraquinone derivative.

The **(3)** was tested to determine their antimicrobial activity against Gram-positive and -negative bacteria, using the agar dilution method according to clinical and laboratory standards institute (formerly CLSI) (CLSI, 2012). The antimycotic effect of the anthraquinone against yeast and fungi was examined with MIC using the broth macro-dilution method according to CLSI (CLSI, 2008).

The authors classified the biological results of the compounds based on susceptibility tests that produce MICs in the range of 100–1000 µg/ml. The antimicrobial activity was considered as significant at 100 µg/ml or less; moderate at 100–500 µg/ml; weak at 500–1000 µg/ml and inactive above 1000 µg/ml according to the MIC results (Ibis et al., 2013).

The derivate was demonstrated to be of effectiveness in different concentrations against Gram-positive and -negative bacteria. The results of the antibacterial activities showed that the significant MIC value was observed against *S. aureus* and *S. epidermidis* (63 and 75 µg/ml, respectively) and the weak MIC value was observed against *B. subtilis* (510 µg/ml). It was observed that the derivate has no activity on *E. faecalis E. coli, K. pneumoniae, P. aeruginosa* and *S. enteritidis*.

The result concerning the *in vitro* antimicrobial activity of the compound with MIC values is presented in Table 1.

The effectiveness of the anthraquinone derivative, **(3)**, was recorded in different concentrations against yeast and fungi. The activity was significant against all tested yeasts and fungi. The highest effectiveness of yeast was shown against *C. albicans* at 15.93 µg/ml concentrations. The effectiveness against *M. canis* and *T. mentagrophytes* was shown at 255 µg/ml concentrations.

The result concerning the *in vitro* antimycotic activity of the **(3)** is presented in Table 2.

According to the xCELLigence analysis of MSCs, any statistically significant difference has not been detected between control and experiment groups for 0.1, 1 and 10 µM concentrations for the all-time points of the analysis. 100 µM concentration caused a delay at cell proliferation for the first 24 h. However, after 24 h, cells had been started to proliferate, and after another 24 h, 100 µM curves reached same values with the other experiment groups (see Figure 4, orange

line). For the 1 mM samples, almost all cells were lost within about half an hour and no proliferation was observed during the experiment (see Figure 4, red curve).

For the WST-1 analysis of MSCs, 100 µM was selected as a medium concentration range; therefore, 10, 50, 100, 200, 500 and 1000 µM concentrations were used. At the end of the experiment, it has been detected that cells were alive up to 100 µM concentration; however, there was a significant decrease for the number of living cells for the concentrations higher than 100 µM.

According to the xCELLigence analysis made on A549s with the concentrations of 10, 50, 100, 200 and 500 µM, it has been observed that compound **(3)** increased proliferation of the cancer cells for all concentrations compared to the controls (Figure 5). However, there was only a significant difference between the control group and 50 µM concentration. At the 72-h WST analysis, no significant vitality differences were detected for the 10, 50, 100 and 200 µM concentrations. However, some vitality loss was observed at 500 µM concentration.

3.1. Structural parameters and vibrational analysis

Although there is no X-ray crystallographic study on the investigated new compound, there are crystal data for related compounds available, as 1-hydroxy-4-propyloxy-9,10-anthraquinone (Nakagawa & Kitamura, 2017) and 1-(piperidin-1-yl)-9,10-anthraquinone (Wnuk, Niedziałkowski, Trzybiński, & Ossowski, 2012). The structural parameters of the lowest-energy conformer of the (3) are given in Table 3, in comparison to the relevant data. It is shown in Table 3 that most of the calculated geometrical parameters of the anthraquinone moiety of the title compound in gas phase are slightly higher or lower than corresponding crystal phase values (Nakagawa & Kitamura, 2017; Wnuk et al., 2012) but are in overall good agreement with the available experimental results.

The vibrational wavenumbers obtained from the experimental IR spectra of solid anthraquinone derivative (3), together with the calculated harmonic vibrational
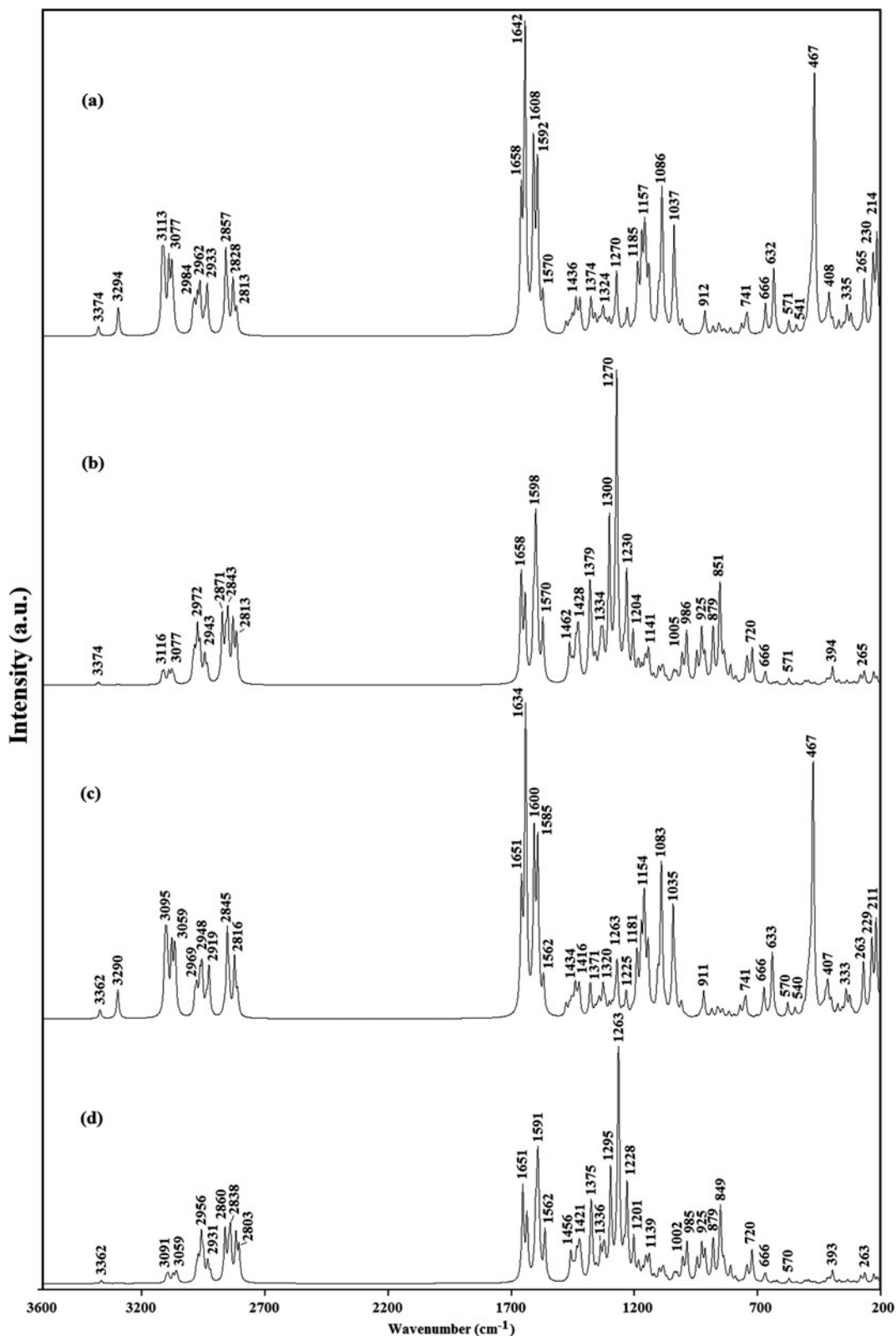
Figure 7. Calculated Raman (a, c) and IR (b, d) spectra of new anthraquinone derivative (3), using DFT/B3LYP/6-31++G(d,p) (a,b), and DFT/B3LYP/6-311++G(d,p) (c, d) levels of theory.

wavenumbers of the most stable conformer, IR and Raman intensities and PED, are shown in Table 4. The natural internal coordinates are given as supplementary file, Table S1.

The experimental and theoretical Raman spectra of 9,10 anthraquinone were investigated by Gribov, Zubkova, and Sigarev (1993), Ball, Zhou, and Liu (1996) and Berezin, Krivokhizhina, and Nechaev (2004). For comparison, the experimental and theoretical vibrational wavenumbers of 9,10-anthraquinone molecule, taken from Gribov et al. (1993), are included in Table 4.
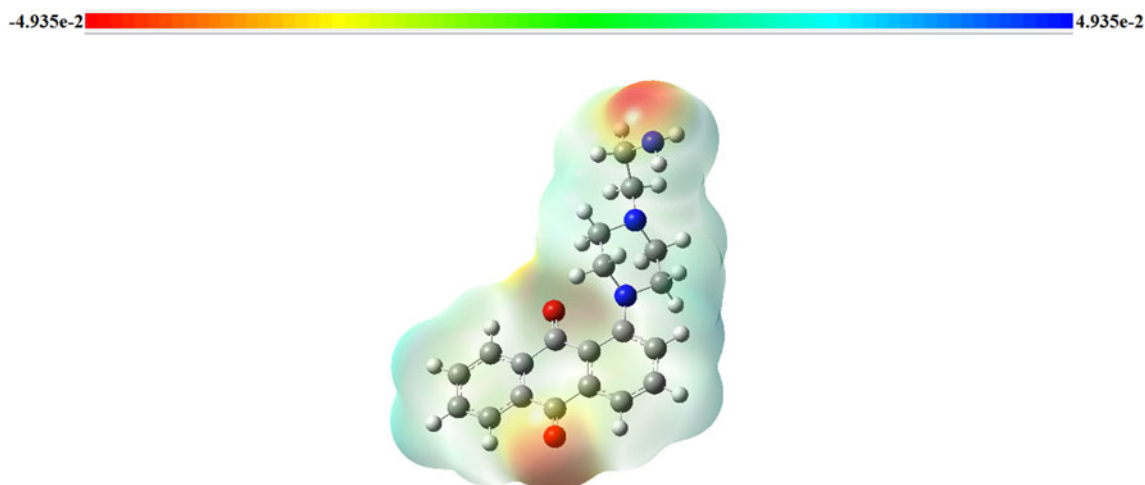
Figure 8. Molecular electrostatic potential energy surface (MEP) for a new anthraquinone derivative calculated with DFT/B3LYP/6-311++G(d,p).

The experimental IR spectrum of the title molecule is shown in Figure 6 and the simulated IR and Raman spectra of the new anthraquinone derivative are shown in Figure 7.

The N–H stretching vibrations appear within the 3500–3000 cm^{-1} region. In a study conducted by Awasthi, Vatsal, and Sharma (2018) on some anthraquinone series of compounds with sulfonamide feature, the N–H stretching wavenumber was observed in the 3431–3232 cm^{-1} region. In another study on anthraquinone derivatives, Beckford and Dixon (2012) assigned the 3338 cm^{-1} band in the IR spectrum to N–H stretching mode. In this study, the N–H stretching modes were computed at 3374, 3362 and 3294, and 3290 cm^{-1} using 6-31++G(d,p) and 6-311++G(d,p) basis sets. These modes were predicted at 3478–3371 cm^{-1} (ν_a NH$_2$) and 3238 cm^{-1} (ν_s NH$_2$) by band component analysis of the 3750–3000 cm^{-1} region of the IR spectrum (see Figure 6). Our results are compatible with the previous findings.

The characteristic region for C–H stretching vibrations is 3100–2800 cm^{-1}. The C–H stretching modes of the investigated molecule were calculated within 3098–2803 cm^{-1} and were observed at 3133, 3029, 2957, 2918 and 2852 cm^{-1} in the IR spectrum. These modes were experimentally observed around 3081–3075 and 3068–3067 cm^{-1} (Ball et al., 1996; Gribov et al., 1993) in the IR spectrum of 9,10-anthraquinone. The computed values, using force field refinement method, were reported as 3068, 3061, 3059 and 3057 cm^{-1} (Gribov et al., 1993) and using BLYP/6-31G* method at 3140, 3139, 3138, 3137, 3118 and 3103 cm^{-1} (Ball et al., 1996). Krishnakumar and Xavier (2005) observed the CH stretching vibrations within 3099–3011 cm^{-1} for 1,4-diaminoanthraquinone. In a study conducted by Celik, Albayrak, Akyuz, and Ozel (2018) on ionic liquids, the aliphatic C–H stretching modes were estimated in the range of 3069–2893 cm^{-1} by DFT/wb97xd/6-31G (d,p) method.

The wavenumbers of the HNH bending vibrational mode were calculated as 1598 cm^{-1} for the title molecule (3) and were predicted at 1629 cm^{-1} by band component analysis of the 1680–1300 cm^{-1} region of the IR spectrum. The wavenumbers of this mode were calculated as 1715 and 1691 cm^{-1} and observed at 1715 and 1718 cm^{-1} for the
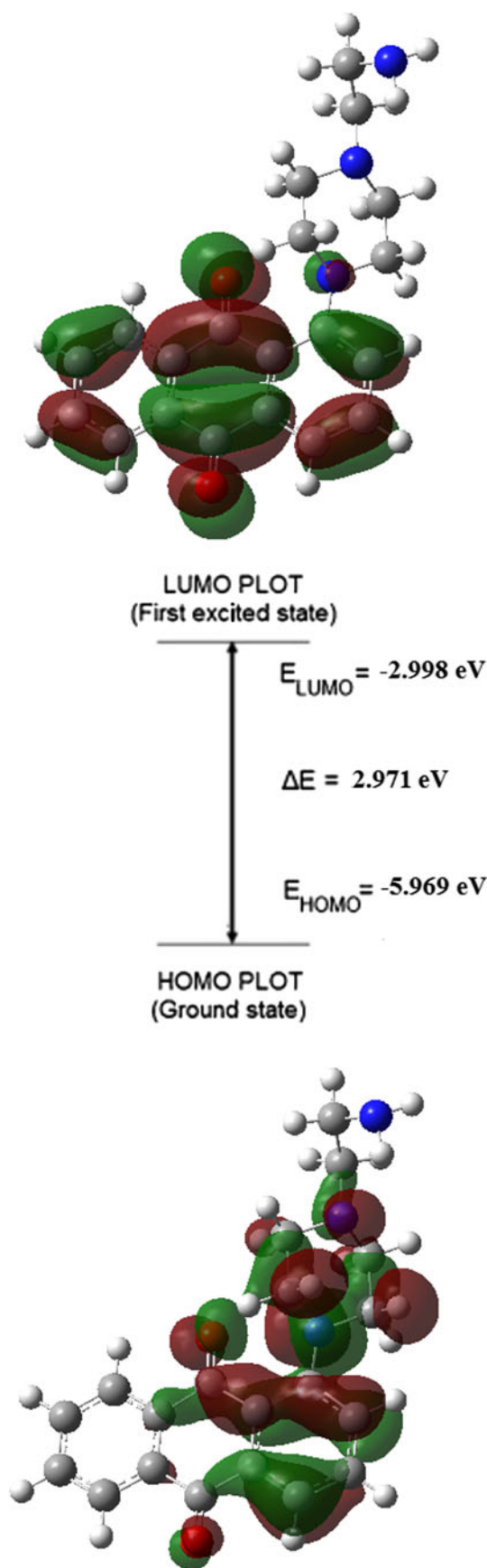
experimental IR and Raman spectra of cyclo(GRGDSPA) (Celik, Kecel-Gunduz, Akyuz, & Ozel, 2018), and in the study conducted by Padmaja, Ravikumar, James, Jayakumar, and Joe (2008), the NH$_3^+$ bending modes of zwitterionic form of L-alanylglycine dipeptide were calculated at about 1599 and 1610 cm^{-1}.

The C=O stretching vibration usually occurs at 1730–1660 cm^{-1} region (Mary, Ushakumari, Harikumar, Varghese, & Panicker, 2009; Padmaja et al., 2008; Roeges, 1994) as a very strong band. The medium intense band appeared at 1668 cm^{-1} in the IR spectrum of our compound was assigned to the C=O stretching vibration. The calculated values corresponding to C=O stretching modes are at 1651 and 1634 cm^{-1}, with PED contributions of 51 and 37%, respectively. The C=O stretching mode of 9, 10-anthraquinone was observed in the experimental spectrum at 1681 cm^{-1} by Gribov et al., (1993) and 1665 cm^{-1} by Ball et al. (1996). In a study conducted by Berezin et al. (2004) on 9,10-anthraquinone, the C=O stretching mode was calculated as 1672 cm^{-1} by B3LYP/6-31G(d) method.

The C–N stretching mode was assigned to the 1156 cm^{-1}(IR) band. The computed wavenumber for this mode was 1154 cm^{-1} with a PED contribution of 36% ν_{CN}. The DFT calculations show that the wavenumbers of mixed vibrations, which have 36, 35, 39, 20, 7 and 12% C–N stretching mode contributions, are 1154, 1139, 1118, 1078, 1002 and 985 cm^{-1}. The corresponding modes were observed at 1055 (IR)–1049 cm^{-1} (Ra), 1218 (IR), 1323 (IR), 1173 (IR)–1120 (Ra) and 1268 (IR)–1294 cm^{-1}(Ra) for piperazine (Gunasekaran & Anita, 2008).

HCH bending vibrational modes were calculated in the interval of 1448–1416 cm^{-1}. This mode was observed at 1360 (IR), 1426 (IR)–1448 (Ra), 1390 (IR) and 1364 cm^{-1} (IR) for piperazine (Gunasekaran & Anita, 2008). The HCH bending modes were observed at 1444 (IR) and 1457 cm^{-1}(Ra) for cyclo(Gly–Gly) and 1458–1467 (IR) and 1470 cm^{-1}(Ra) for cyclo(L-Ser–L-Ser) dipeptides (Mendham, Dines, Snowden, Chowdhry, & Withnall, 2009a,Mendham, Dines, Snowden, Withnall, & Chowdhry, 2009b).

LUMO PLOT
(First excited state)

$E_{LUMO} = -2.998$ eV

$\Delta E = 2.971$ eV

$E_{HOMO} = -5.969$ eV

HOMO PLOT
(Ground state)

Figure 9. The atomic orbital HOMO–LUMO composition of the frontier molecular orbital for new anthraquinone derivative, calculated with DFT/B3LYP/6-311++G(d,p).

3.2. Molecular electrostatic potential (MEP)

The MEP surface of the new anthraquinone derivative, changing from -1.343 V (darkest red) to 1.343 V (deepest blue), is shown in Figure 8.

The blue color indicates nucleophilic reactivity, while the red color indicates electrophilic reactivity. According to these calculations, the MEP map shows that the regions with negative potential are concentrated on oxygen and the regions with positive potentials are concentrated on the hydrogen atoms of the NH and CH groups.

3.3. Highest occupied molecular orbital (HOMO) and lowest occupied molecular orbital (LUMO) energies

The frontier molecular orbitals play an important role in the chemical reactions, electric and optical properties, and UV–vis spectra. The HOMO and LUMO energies of new anthraquinone derivative are calculated by DFT method at B3LYP/6-311++G(d,p) level of theory.

The HOMO–LUMO energy gap is the measure of the kinetic stability and reactivity of the compounds. The lower gap between HOMO and LUMO energies of a compound suggests its higher reactivity (Pearson, 1973). In a study conducted by Awasthi et al. (2018), the HOMO–LUMO energy gaps in a series of anthraquinone compounds were compared and correlated to their biological activity. Kumar et al. (2015) calculated the HOMO–LUMO energy separation of phomarin, a naturally occurring anthraquinone, as 3.824 eV. In that study, phomarin was shown to have remarkable biological activities against malaria parasite. The HOMO–LUMO energy separation in the title compound was found to be 2.971 eV (0.10918 a.u.), and the compounds with smaller HOMO–LUMO energy separations can be predicted to have a greater biological activity (Patra, Paul, Sepay, Kundu, & Ghosh, 2018).

The frontier molecular orbitals (HOMO and LUMO) are shown in Figure 9.

3.4. Docking studies

Anthraquinones form the building block of some anticancer drugs and perform their cytotoxic activities by their interaction with DNA and by inhibition of topoisomerase II activity (Al-Otaibi, Spittle, & El Gogary, 2017). Ansari, Khan, and Naqvi (2018) investigated the interaction of two anthraquinones, i.e. danthron and quinizarin with human serum albumin (HSA) and found that both drugs effectively bind HSA and form a stable drug–protein complex. It was also reported that van der Waals forces, hydrophobic forces and electrostatic forces played a vital role in the stabilization of drug––protein complex formed (Ansari et al., 2018).

The 1,4-dihydroxy-9,10-anthraquinone molecule, which is an analogue of the basic unit of anthracycline anticancer drugs, interacts with the calf thymus DNA. This is one of the reasons why the 1,4-dihydroxy-9,10-anthraquinone molecule, which has a smaller structure compared to anthracyclines, has a high binding constant (Guin, Das, & Mandal, 2011).
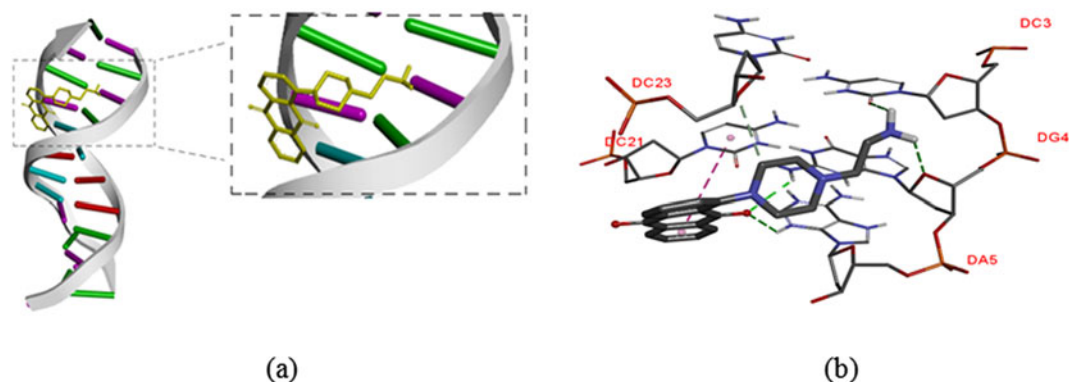
Figure 10. (a) Docking of anthraquinone derivative with DNA. (b) The detailed interactions of the optimized structure of anthraquinone derivative in gas phase with the DNA; dotted lines represent the interactions.

The docking analysis of anthraquinone derivative was performed using the AutoDock-Vina program (Trott & Olson, 2010). The crystal structure of DNA was obtained from the protein data bank (PDB ID: 1BNA) (Drew et al., 1981). The DNA was adapted for docking by removing water molecules and adding polar hydrogens. Kollman charges of DNA were calculated. The anthraquinone derivative in the gas phase was optimized and made ready for the docking process. The partial charges of the molecule were also determined using the Geisinger method. The active site of DNA was defined in the grid size of 40 Å × 40 Å × 40 Å. The anthraquinone derivative binds to the active site of DNA by hydrogen bonding interactions (Figure 10). The optimized structure of the molecule, which was calculated by DFT/B3LYP/6-311++G(d,p) in the gas phase, is bound to the DC3, DG4, DA5, DC21 and DC23 residues of DNA via the intermolecular hydrogen bonds. It follows that the docked ligand formed a stable complex with DNA. The results reveal that the binding affinity (ΔG) value is −8.0 in kcal/mol.

4. Conclusion

In the current study, the examination of the antibacterial activities of new anthraquinone derivative against Gram-positive and Gram-negative bacteria determines that the highest effectiveness was against *S. aureus* and *S. epidermidis*, while there was no activity against Gram-negative bacteria. *Antimycotic activity is also examined and the highest effectiveness has been shown against C. albicans.*

As a conclusion, it is thought that this new anthraquinone derivate can be used as a therapeutic agent because of its effective and useful antibacterial and antimycotic activities, in the treatment of infections caused by *Staphylococcus* and *Candida* species.

According to cellular analysis, it has been observed that 100 μM concentration of compound **(3)** can delay proliferation of the healthy MSCs for 24 h; however, this delay is temporary, and after 72 h, there was no significant difference between the 100 μM sample and control sample. However, a 10-fold concentration (1 mM) caused a catastrophic decrease on cell viability. Thus, high doses of the compound were found to be not compatible with the healthy human cells for industrial or medical purposes. Lower doses than 100 μM may not cause any negative effect on cells. However, more extensive *in vitro* and

in vivo analyses are required to determine the more specific and detailed effects of the compound before its use.

When the effect of the compound on the viability of the cancer cells is examined, it has been shown that the proliferation inhibiting concentrations in healthy cells is better tolerated by the cancer cells and even increased the proliferation of cancer cells at certain concentration (50 μM). This has led to the conclusion that the compound can be used as a proliferation-inducing agent which selectively enhances the proliferation of cancer cells as opposed to healthy cells. Still, further studies are required with different healthy or cancer cell lines to evaluate the effect of the compound for different cell types.

The quantum mechanics and molecular docking calculations have also been performed for the first time in order to determine the new anthraquinone's anticancer activity. The objective of this work was to synthesize and evaluate the structural formulation, characterization, antimicrobial activity and cytotoxicity analysis of [1-(2-Aminoethyl)piperazinyl-9,10-dioxo-anthraquinone], which is expected to replace anthracyclines in the future.

References

Al-Otaibi, J. S., Spittle, P. T., & El Gogary, T. M. (2017). Interaction of anthraquinone anti-cancer drugs with DNA: Experimental and computational quantum chemical study. *Journal of Molecular Structure*, *1127*, 751–760. doi:10.1016/j.molstruc.2016.08.007

Ansari, S. S., Khan, R. H., & Naqvi, S. (2018). Probing the intermolecular interactions into serum albumin and anthraquinone systems: A spectroscopic and docking approach. *Journal of Biomolecular Structure and Dynamics*, *36*(13), 3362–3375. doi:10.1080/07391102.2017.1388284

Awasthi, P., Vatsal, M., & Sharma, A. (2018). Structural and biological study of synthesized anthraquinone series of compounds with sulfonamide feature. *Journal of Biomolecular Structure and Dynamics*, 1–46. doi:10.1080/07391102.2018.1552198

Ball, B., Zhou, X., & Liu, R. (1996). Density functional theory study of vibrational spectra. 8. Assignment of fundamental vibrational modes of 9, 10-anthraquinone and 9, 10-anthraquinone-d8. *Spectrochimica Acta Part A: Molecular and Biomolecular Spectroscopy*, *52*(14), 1803–1814. doi:10.1016/S0584-8539(96)01769-2

Becke, A. D. (1993). Density-functional thermochemistry. III. The role of exact exchange. *The Journal of Chemical Physics*, *98*(7), 5648–5652. doi:10.1063/1.464913

Beckford, S. J., & Dixon, D. W. (2012). Molecular dynamics of anthraquinone DNA intercalators with polyethylene glycol side chains. *Journal of Biomolecular Structure & Dynamics*, *29*(5), 1065–1080. doi:10.1080/073911012010525031

Berezin, K. V., Krivokhizhina, T. V., & Nechaev, V. V. (2004). Atypical intensity distribution in the Raman spectrum of 9, 10-anthraquinone. *Optics and Spectroscopy*, *97*(4), 530–536. doi:10.1134/1.1813693

Celik, S., Ozel, A. E., Akyuz, S., Ozkok, F., Sahin, Y. M., Sıgırcı, B. D., … Karaoz, E. (2018). *Antibakteriyel ve antimikotik etki arz eden amino antrakinon analoğu ve bunun moleküler modellemesi, Patent, TR 2018/06753*. Turkey.

Celik, S., Kecel-Gunduz, S., Akyuz, S., & Ozel, A. E. (2018). Structural analysis, spectroscopic characterization and molecular docking studies of the cyclic heptapeptide. *Journal of Biomolecular Structure and Dynamics*, *36*(9), 2407–2423. doi:10.1080/07391102.2017.1356240

Celik, S., Albayrak, A. T., Akyuz, S., & E. Ozel, A. (2018). Molecular modelling and vibrational investigations of ammonium-based ionic liquid (CLTOAB). *Journal of Biomolecular Structure and Dynamics*, 1–12. doi:10.1080/07391102.2018.1495578

CLSI. (2008). *Reference method for broth dilution antifungal susceptibility testing of filamentous fungi; approved standard CLSI document M38-A2*. Wayne, PA: Clinical and Laboratory Standards Institute.

CLSI. (2012). *Methods for dilution antimicrobial susceptibility tests for bacteria that grow aerobically; approved standard – (9th Ed.), M07-A9*. Wayne, PA: Clinical and Laboratory Standards Institute.

Cudlin, J., Blumauerova, M., Steinerova, N., Mateju, J., & Zalabak, V. (1976). Biological activity of hydroxyanthraquinones and their glucosides toward microorganisms. *Folia Microbiology*, *21*, 54–57.

Drew, H. R., Wing, R. M., Takano, T., Broka, C., Tanaka, S., Itakura, K., & Dickerson, R. E. (1981). Structure of a B-DNA dodecamer: Conformation and dynamics. *Proceedings of the National Academy of Sciences*, *78*(4), 2179–2183.

Driscoll, J. S., Hazard, G. F., Wood, H. B., & Goldin, A. (1974). Structure–antitumor activity relationships among quinone derivatives. *Cancer Chemotherapy Reports 2*, *4*(2), 1–362.

Fain, V. Y. (1999). *9,10-Antrakhinony i ikh primenenie (9,10-Anthraquinines and their application)*. Moscow: Tsentr Fotokhimii Ross. Akad. Nauk.

Frisch, M. J., Trucks, G. W., Schlegel, H. B., Scuseria, G. E., Robb, M. A., Cheeseman, J. R., … Pople, J. A. (2004). *Gaussian 03, Revision C. 02*. Wallingford CT: Gaussian, Inc.

Gribov, L. A., Zubkova, O. B., & Sigarev, A. A. (1993). Theoretical analysis of infrared spectrum of 9, 10-anthraquinone molecule. *Journal of Structural Chemistry*, *34*(1), 147–154. doi:10.1007/BF00745414

Guin, P. S., Das, S., & Mandal, P. C. (2011). Interaction of 1, 4-dihydroxy–9, 10-anthraquinone with calf thymus DNA: A comparison with anthracycline anticancer drugs. *Journal of Solution Chemistry*, *40*(3), 492–501. doi:10.1007/s10953-011-9654-x

Gunasekaran, S., & Anita, B. (2008). Spectral investigation and normal coordinate analysis of piperazine. *Indian Journal of Pure & Applied Physics*, *46*(12), 833–838.

IARC Working Group on the Evaluation of Carcinogenic Risks to Humans (2013). Some chemicals present in industrial and consumer products, food and drinking-water. *IARC Monographs on the Evaluation of Carcinogenic Risks to Humans*, *101*, 9.

Ibis, C., Tuyun, A. F., Bahar, H., Ayla, S. S., Stasevych, M. V., Musyanovych, R. Y., … Novikov, V. (2013). Synthesis of novel 1, 4-naphthoquinone derivatives: Antibacterial and antifungal agents. *Medicinal Chemistry Research*, *22*(6), 2879–2888. doi:10.1007/s00044-012-0300-y

Istvan, K. (2002). *Simirra, A program for simulation of IR and Raman spectra*. Budapest: Chemical Research Center (It was obtained from Dr. Gabor Keresztury in Chemical Research Center in Budapest).

Krishnakumar, V., & Xavier, R. J. (2005). Vibrational analysis of 1, 4-diaminoanthraquinone and 1, 5-dichloroanthraquinone: A joint FTIR, FT–Raman and scaled quantum mechanical study. *Spectrochimica Acta Part A: Molecular and Biomolecular Spectroscopy*, *61*(8), 1799–1809. doi:10.1016/j.saa.2004.07.011

Kumar, A., Srivastava, A. K., Gangwar, S., Misra, N., Mondal, A., & Brahmachari, G. (2015). Combined experimental (FT-IR, UV–visible spectra, NMR) and theoretical studies on the molecular structure, vibrational spectra, HOMO, LUMO, MESP surfaces, reactivity descriptor and molecular docking of Phomarin. *Journal of Molecular Structure*, *1096*, 94–101. doi:10.1016/j.molstruc.2015.04.031

Mary, Y. S., Ushakumari, L., Harikumar, B., Varghese, H. T., & Panicker, C. Y. (2009). FT-IR, FT-Raman and SERS spectra of L-proline. *Journal of the Iranian Chemical Society*, *6*(1), 138–144. doi:10.1007/BF03246512

Mendham, A. P., Dines, T. J., Snowden, M. J., Chowdhry, B. Z., & Withnall, R. (2009a). Vibrational spectroscopy and DFT calculations of di-amino acid cyclic peptides. Part I: Cyclo (Gly-Gly), cyclo (L-Ala-L-Ala) and cyclo (L-Ala-Gly) in the solid state and in aqueous solution. *Journal of Raman Spectroscopy*, *40*(11), 1478–1497. doi:10.1002/jrs.2293

Mendham, A. P., Dines, T. J., Snowden, M. J., Withnall, R., & Chowdhry, B. Z. (2009b). IR/Raman spectroscopy and DFT calculations of cyclic di-amino acid peptides. Part III: Comparison of solid state and solution structures of cyclo (L-Ser-L-Ser). *Journal of Raman Spectroscopy*, *40*(11), 1508–1520. doi:10.1002/jrs.2306

Nakagawa, H., & Kitamura, C. (2017). Crystal structures of 1-hydroxy-4-propyloxy-9, 10-anthraquinone and its acetyl derivative. *Acta Crystallographica Section E Crystallographic Communications*, *73*(12), 1845–1849. doi:10.1107/S2056989017015973

Nollet, L. M. L., & Gutierrez-Uribe, J. A. (2018). *Phenolic compounds in food characterization and analysis* (pp. 1–430). Boca Raton, FL: CRC Press.

Ozkok, F., & Sahin, Y. M. (2016). *Bioaktif Antrakinon Anologlarının Sentezine Yönelik Özgün Metot Geliştirilmesi, Patent, TR 2016/19610*. Turkey.

Padmaja, L., Ravikumar, C., James, C., Jayakumar, V. S., & Joe, I. H. (2008). Analysis of vibrational spectra of l-alanylglycine based on density functional theory calculations. *Spectrochimica Acta Part A: Molecular and Biomolecular Spectroscopy*, *71*(1), 252–262. doi:10.1016/j.saa.2007.12.019

Patra, D., Paul, S., Sepay, N., Kundu, R., & Ghosh, T. (2018). Structure–activity relationship on DNA binding and anticancer activities of a family of mixed-ligand oxidovanadium(V) hydrazone complexes. *Journal of Biomolecular Structure and Dynamics*, *36*(16), 4143–4155. doi:10.1080/07391102.2017.1409652

Pearson, R. G. (1973). *Hard and soft acids and bases* (Vol. 2). New York, NY: Van Nostrand Reinhold.

Pulay, P., Fogarasi, G., Pongor, G., Boggs, J. E., & Vargha, A. (1983). Combination of theoretical ab initio and experimental information to obtain reliable harmonic force constants. Scaled quantum mechanical (QM) force fields for glyoxal, acrolein, butadiene, formaldehyde, and ethylene. *Journal of the American Chemical Society*, *105*(24), 7037–7047. doi:10.1021/ja00362a005

Roeges, N. P. (1994). *A guide to the complete interpretation of infrared spectra of organic structures*. New York, NY: Wiley.

Schinazi, R. F., Chu, C. K., Babu, J. R., Oswald, B. J., Saalmann, V., Cannon, D. L., … Nasr, M. (1990). Anthraquinones as a new class of antiviral agents against human immunodeficiency virus. *Antiviral Research*, *13*(5), 265–272. doi:10.1016/0166-3542(90)90071-E

Sendelbach, L. E. (1989). A review of the toxicity and carcinogenicity of anthraquinone derivatives. *Toxicology*, *57*(3), 227–240.

Shao, Y., Molnar, L. F., Jung, Y., Kussmann, J., Ochsenfeld, C., Brown, S. T., … Head-Gordon, M. (2006). Advances in methods and algorithms in a modern quantum chemistry program package. *Physical Chemistry Chemical Physics*, *8*(27), 3172–3191.

Sundius, T. (1990). Molvib – A flexible program for force field calculations. *Journal of Molecular Structure*, *218*, 321–326. doi:10.1016/0022-2860(90)80287-T

Sundius, T. (2002). Scaling of ab initio force fields by MOLVIB. *Vibrational Spectroscopy*, *29*(1-2), 89–95. doi:10.1016/S0924-2031(01)00189-8

Trott, O., & Olson, A. J. (2010). AutoDock Vina: Improving the speed and accuracy of docking with a new scoring function, efficient optimization, and multithreading. *Journal of Computational Chemistry*, *31*(2), 455–461. doi:10.1002/jcc.21334

Windholtz, M., Budavari, S., Stroumtsos, L. Y., & Fertig, M. N. (1976). *Merck Index, An encyclopedia of chemicals and drugs* (Vol. 94). Kenilworth, NJ: Merck Index & Co. Inc.

Wnuk, E., Niedziałkowski, P., Trzybiński, D., & Ossowski, T. (2012). 1-(Piperidin-1-yl)-9,10-anthraquinone. *Acta Crystallographica. Section E, Structure Reports Online*, *68*(Pt 10), o2879. doi:10.1107/S1600536812037713